Sleep Drives Metabolite Clearance from the Adult Brain

Lulu Xie,[1]* Hongyi Kang,[1]* Qiwu Xu,[1] Michael J. Chen,[1] Yonghong Liao,[1] Meenakshisundaram Thiyagarajan,[1] John O'Donnell,[1] Daniel J. Christensen,[1] Charles Nicholson,[2] Jeffrey J. Iliff,[1] Takahiro Takano,[1] Rashid Deane,[1] Maiken Nedergaard[1]†

The conservation of sleep across all animal species suggests that sleep serves a vital function. We here report that sleep has a critical function in ensuring metabolic homeostasis. Using real-time assessments of tetramethylammonium diffusion and two-photon imaging in live mice, we show that natural sleep or anesthesia are associated with a 60% increase in the interstitial space, resulting in a striking increase in convective exchange of cerebrospinal fluid with interstitial fluid. In turn, convective fluxes of interstitial fluid increased the rate of β-amyloid clearance during sleep. Thus, the restorative function of sleep may be a consequence of the enhanced removal of potentially neurotoxic waste products that accumulate in the awake central nervous system.

Despite decades of effort, one of the greatest mysteries in biology is why sleep is restorative and, conversely, why lack of sleep impairs brain function (*1*, *2*). Sleep deprivation reduces learning, impairs performance in cognitive tests, prolongs reaction time, and is a common cause of seizures (*3*, *4*). In the most extreme case, continuous sleep deprivation kills rodents and flies within a period of days to weeks (*5*, *6*). In humans, fatal familial or sporadic insomnia is a progressively worsening state of sleeplessness that leads to dementia and death within months or years (*7*).

Proteins linked to neurodegenerative diseases, including β-amyloid (Aβ) (*8*), α-synuclein (*9*), and tau (*10*), are present in the interstitial space surrounding cells of the brain. In peripheral tissue, lymph vessels return excess interstitial proteins to the general circulation for degradation in the liver (*11*). Yet despite its high metabolic rate and the fragility of neurons to toxic waste products, the brain lacks a conventional lymphatic system. Instead, cerebrospinal fluid (CSF) recirculates through the brain, interchanging with interstitial fluid (ISF) and removing interstitial proteins, including Aβ (*12*, *13*). The convective exchange of CSF and ISF is organized around the cerebral vasculature, with CSF influx around arteries, whereas ISF exits along veins. These pathways were named the glymphatic system on the basis of their dependence on astrocytic aquaporin-4 (AQP4) water channels and the adoption of functions homologous to peripheral lymphatic removal of interstitial metabolic byproducts (*14*). Deletion of AQP4 channels reduces clearance of exogenous Aβ by 65%, suggesting that convective movement of ISF is a substantial contributor to the removal of interstitial waste products and other products of cellular activity (*12*). The interstitial concentration of Aβ is higher in awake than in sleeping rodents and humans, possibly indicating that wakefulness is associated with increased Aβ production (*15*, *16*). We tested the alternative hypothesis that Aβ clearance is increased during sleep and that the sleep-wake cycle regulates glymphatic clearance.

We used in vivo two-photon imaging to compare CSF influx into the cortex of awake, anesthetized, and sleeping mice. The fluorescent tracers were infused into the subarachnoid CSF via a cannula implanted in the cisterna magna for real-time assessment of CSF tracer movement. Electrocorticography (ECoG) and electromyography (EMG) were recorded in order to continuously monitor the state of brain activity (Fig. 1A and fig. S1). In initial experiments, the volume and rate of tracer infusion were adjusted so as to avoid changes in behavior state or ECoG (fig. S1). Because mice sleep much of the day, a small molecular weight tracer, fluorescein isothiocyanate (FITC)–dextran (3 kD) in aCSF, was infused at midday (12 to 2 p.m.) via the cannula implanted in the cisterna magna. In sleeping mice, a robust influx of the fluorescent CSF tracer was noted along periarterial spaces, in the subpial regions, and in the brain parenchyma similar to previous findings in anesthetized mice (Fig. 1, B and C, and fig. S2) (*12*). ECoG power spectrum analysis depicted a relatively high power of slow waves that is consistent with sleep (Fig. 1D). CSF tracer infusion (Texas red-dextran, 3 kD) was repeated in the same mouse after it was awakened through gentle handling of its tail. Unexpectedly, arousal sharply reduced tracer influx compared with that of the sleeping state. Periarterial and parenchymal tracer influx was reduced by ~95% in awake as compared with sleeping mice during the 30-min imaging session (Fig. 1, B and C, and fig. S2). ECoG showed a reduction in the relative prevalence of slow (delta) waves concomitant with a significant increase in the power of fast activity, confirming that the animals were awake ($n = 6$ mice, $P < 0.05$, paired t test) (Fig. 1D). To investigate whether the state of brain activity indeed controlled CSF influx, we repeated the experiments in a new cohort of mice in which all experiments were performed when the animals were awake (8 to 10 p.m.). Because mice normally do not sleep at this time of day, we first evaluated CSF tracer influx in the awake state by means of intracisternal infusion of FITC-dextran. CSF tracer influx into the brain was largely absent and only slowly gained access to the superficial cortical layers (Fig. 1, E and F, and fig. S2). After 30 min imaging of CSF tracer in the awake state, the animals were anesthetized with intraperitoneal administration of ketamine/xylazine (KX). Texas red-dextran was administered 15 min later, when a stable increase in slow wave activity was noted (Fig. 1, E and F). Texas red-dextran rapidly flushed in along periarterial spaces and entered the brain parenchyma at a rate comparable with that of naturally sleeping mice (Fig. 1, B and E). Ketamine/xylazine anesthesia significantly increased influx of CSF tracer in all mice analyzed [$n = 6$ mice, $P < 0.05$, two-way analysis of variance (ANOVA) with Bonferroni test], which was concomitant with a significant increase in the power of slow wave activity ($n = 6$ mice, $P < 0.05$, paired t test) (Fig. 1, G and F). Thus, glymphatic CSF influx is sharply suppressed in conscious alert mice as compared with naturally sleeping or anesthetized littermates.

Influx of CSF is in part driven by arterial pulse waves that propel the movement of CSF inward along periarterial spaces (*12*). It is unlikely that diurnal fluctuations in arterial pulsation are responsible for the marked suppression of convective CSF fluxes during wakefulness because arterial blood pressure is higher during physical activity. An alternative possibility is that the awake brain state is linked to a reduction in the volume of the interstitial space because a constricted interstitial space would increase resistance to convective fluid movement and suppress CSF influx. To assess the volume and tortuosity of the interstitial space in awake versus sleeping mice, we used the real-time iontophoretic tetramethylammonium (TMA) method in head-fixed mice (Fig. 2A and fig. S3) (*17*, *18*). TMA recordings in cortex of sleeping mice collected at midday (12 to 2 p.m.) confirmed that the interstitial space volume fraction (α) averaged 23.4 ± 1.9% ($n = 6$ mice) (*19*). However, the interstitial volume fraction was only 14.1 ± 1.8% in awake mice recorded at 8 to 10 p.m. ($n = 4$ mice, $P < 0.01$, t test) (Fig. 2B). Analysis of cortical ECoG recorded by the TMA reference electrode confirmed that the power of slow wave activity was higher in sleeping than in awake mice, which is concurrent with a lower power of high-frequency activity (Fig. 2C).

To further validate that the volume of the interstitial space differed in awake versus sleeping mice, we also obtained TMA recordings in awake mice in the late evening (8 to 10 p.m.) and repeated the recordings in the same mice after administration of ketamine/xylazine. This approach,

[1]Division of Glial Disease and Therapeutics, Center for Translational Neuromedicine, Department of Neurosurgery, University of Rochester Medical Center, Rochester, NY 14642, USA. [2]Department of Neuroscience and Physiology, Langone Medical Center, New York University, New York, NY 10016, USA.

*These authors contributed equally to this work.
†Corresponding author. E-mail: nedergaard@urmc.rochester.edu

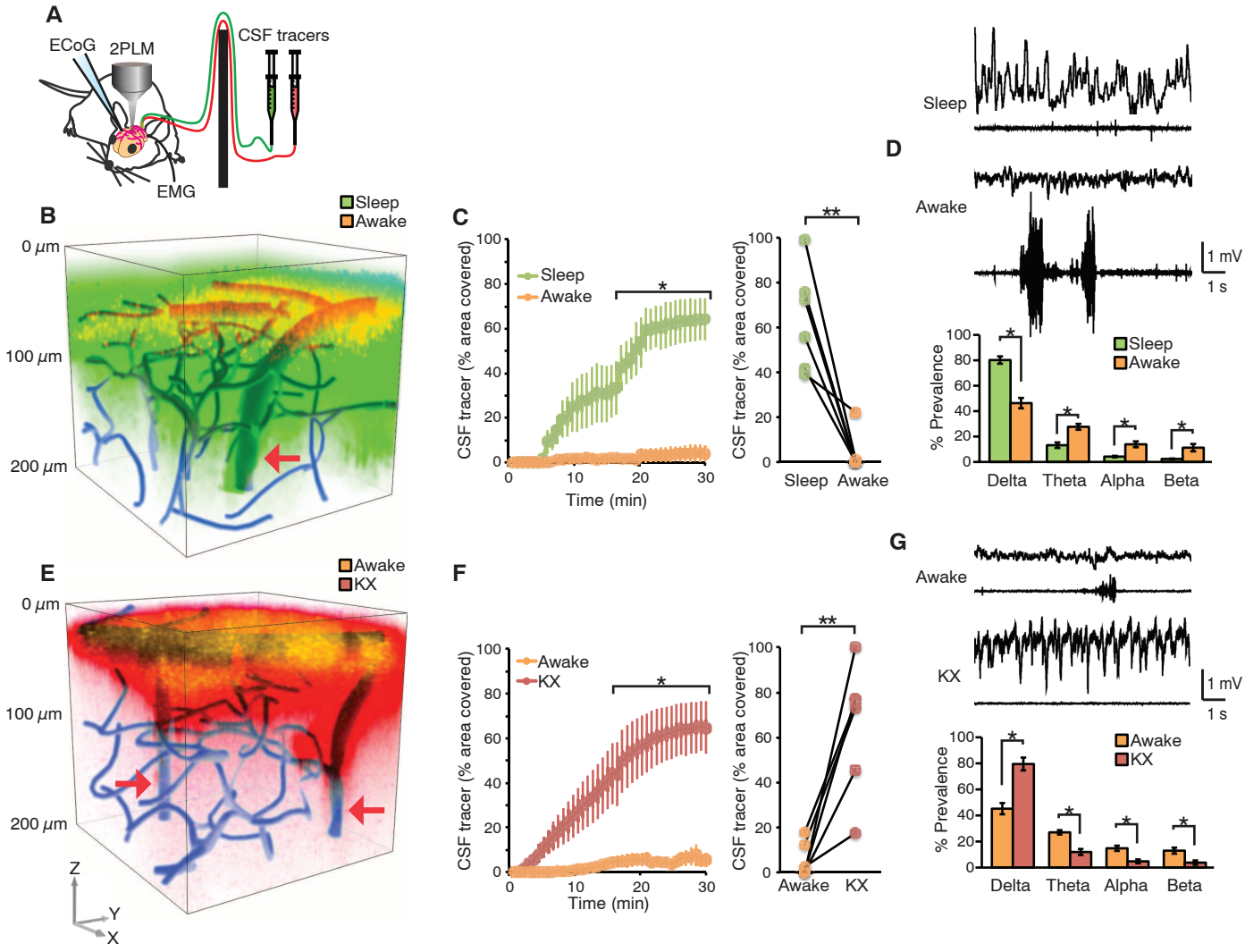

Fig. 1. Wakefulness suppresses influx of CSF tracers. (**A**) Diagram of experimental setup used for two-photon imaging of CSF tracer movement in real time. To avoid disturbing the state of brain activity, a cannula with dual ports was implanted in the cisterna magna for injection of CSF tracers. ECoG and EMG were recorded to monitor the state of brain activity. (**B**) Three-dimensional (3D) vectorized reconstruction of the distribution of CSF tracers injected in a sleeping mouse and then again after the mouse was awakened. The vasculature was visualized by means of cascade blue-dextran administered via the femoral vein. FITC-dextran (green) was first injected in the cisterna magna in a sleeping mouse and visualized by collecting repeated stacks of z-steps. Thirty min later, the mouse was awakened by gently moving its tail, and Texas red-dextran (red) was administered 15 min later. The experiments were performed mostly asleep (12 to 2 p.m.). The arrow points to penetrating arteries. (**C**) Comparison of time-dependent CSF influx in sleep versus awake. Tracer influx was quantified 100 μm below the cortical surface; $n = 6$ mice; $^{*}P < 0.05$, two-way ANOVA with Bonferroni test. (Right) The tracer intensity within the two arousal states at the 30-min time point was compared. $^{**}P < 0.01$, t test. (**D**) ECoG and EMG recordings acquired during sleep and after the mouse was awakened. Power spectrum analysis of all the animals analyzed in the two arousal states ($n = 6$ mice; $^{*}P < 0.05$, t test). (**E**) 3D reconstruction of CSF tracer influx into the mouse cortex. FITC-dextran was first injected in the awake stage, and cortical influx was visualized by means of two-photon excitation for 30 min. The mouse was then anesthetized with ketamine/xylazine (intraperitoneally), and Texas red-dextran was injected intracisternally 15 min later. The vasculature was visualized by means of cascade blue-dextran. Arrows point to penetrating arteries. (**F**) Comparison of time-dependent CSF influx in awake versus ketamine/xylazine anesthesia; $n = 6$ mice; $^{*}P < 0.05$, two-way ANOVA with Bonferroni test. (Right) The tracer intensity during the two arousal states at the 30-min time point was compared. $^{**}P < 0.01$, t test. (**G**) ECoG and EMG recordings in the awake mouse and after administration of ketamine/xylazine. Power spectrum analysis of all the animals analyzed in the two arousal states; $n = 6$ mice; $^{*}P < 0.05$, t test.

which eliminated interanimal variability in electrode placement and TMA calibration, showed that anesthesia consistently increased the interstitial space volume fraction by >60%, from 13.6 ± 1.6% for awake mice to 22.7 ± 1.3% in the same mice after they received ketamine/xylazine ($n = 10$ mice, $P < 0.01$, paired t test) (Fig. 2D). Analysis of ECoG activity extracted from the TMA reference electrode showed that ketamine/xylazine increased the power of slow wave activity in all animals analyzed (Fig. 2E). Thus, the cortical interstitial volume fraction is 13 to 15% in the awake state as compared to 22 to 24% in sleeping or anesthetized mice. Tortuosity of the interstitial space did not differ significantly according to changes in the state of brain activity; awake, sleeping, and anesthetized mice all exhibited a λ value in the range of 1.3 to 1.8, which is consistent with earlier reports ($n = 4$ to 10 mice, $P > 0.1$, t test) (Fig. 2, B and D) (*19*–*21*). Recordings obtained 300 μm below the cortical surface did not differ significantly from those obtained at 150 μm, suggesting that preparation of the cranial window was not associated with tissue injury ($n = 6$ mice, $P > 0.4$, t test) (Fig. 2D and fig. S3D). Other reports have shown that the interstitial volume is ~19% in anesthetized young mice but declines to ~13% in

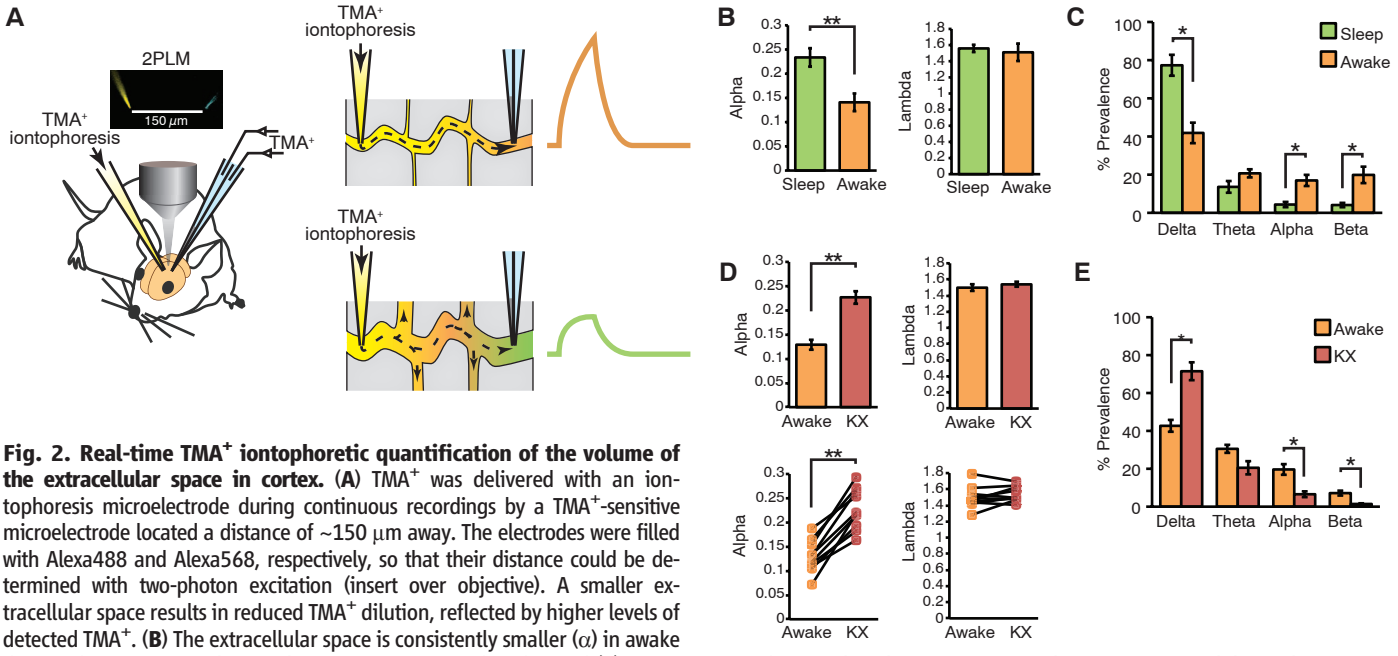

Fig. 2. Real-time TMA$^+$ iontophoretic quantification of the volume of the extracellular space in cortex. (**A**) TMA$^+$ was delivered with an iontophoresis microelectrode during continuous recordings by a TMA$^+$-sensitive microelectrode located a distance of ~150 μm away. The electrodes were filled with Alexa488 and Alexa568, respectively, so that their distance could be determined with two-photon excitation (insert over objective). A smaller extracellular space results in reduced TMA$^+$ dilution, reflected by higher levels of detected TMA$^+$. (**B**) The extracellular space is consistently smaller (α) in awake than in sleeping mice, whereas the tortuosity remained unchanged (λ); $n = 4$ to 6 mice; $^{**}P < 0.01$, *t* test. (**C**) Power spectrum analysis of ECoG recordings; $n = 6$ mice; $^{*}P < 0.05$, *t* test. (**D**) The extracellular space was consistently smaller in the awake state than after administration of ketamine/xylazine in paired recordings within the same mouse, whereas tortuosity did not change after anesthesia; $n = 10$ mice; $^{**}P < 0.01$, *t* test. (Bottom) TMA measurements obtained during the two arousal states compared for each animal. (**E**) Power spectrum analysis of ECoG; $n = 6$ mice; $^{*}P < 0.05$, *t* test.

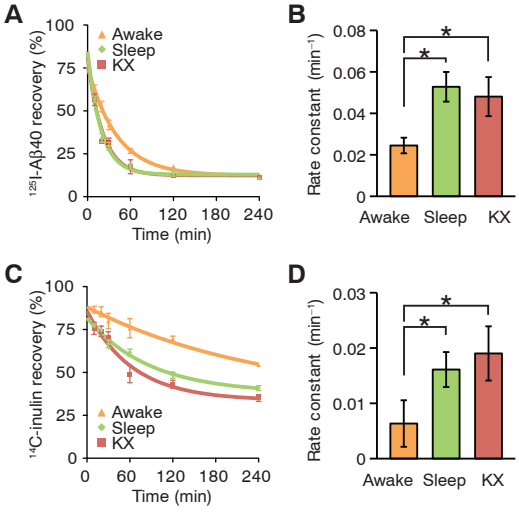

Fig. 3. Sleep improves clearance of Aβ. (**A**). Time-disappearance curves of ^{125}I-Aβ$_{1\text{-}40}$ after its injection into the frontal cortex in awake (orange triangles), sleeping (green diamonds), and anesthetized (red squares, ketamine/xylazine) mice. (**B**) Rate constants derived from the clearance curves. (**C**) Time-disappearance curves of ^{14}C-inulin after its injection into the frontal cortex of awake (orange triangles), sleeping (green diamonds), and anesthetized (red squares, ketamine/xylazine) mice. (**D**) Rate constants derived from the clearance curves. A total of 77 mice were included in the analysis: 25 awake, 29 asleep, and 23 anesthetized, with 3 to 6 mice per time point. $^{*}P < 0.05$ compared with awake, ANOVA with Bonferroni test.

aged mice (*22*). Collectively, these observations support the notion that influx of CSF tracers is suppressed in awake mice as a result of contraction of the interstitial space: The smaller space during wakefulness increases tissue resistance to interstitial fluid flux and inward movement of CSF. This effect of arousal state on interstitial volume likely holds major implications for diffusion of neurotransmitters, such as glutamate (*23*).

Because previous analysis indicates that as much as 65% of exogenously delivered Aβ is cleared by the glymphatic system (*12*), we tested whether interstitial Aβ is cleared most efficiently during sleep. Radiolabeled ^{125}I-Aβ$_{1\text{-}40}$ was injected intracortically in three groups of animals: freely behaving awake mice, naturally sleeping mice, and animals anesthetized with ketamine/xylazine (fig. S4). Brains were harvested 10 to 240 min later for analysis of ^{125}I-Aβ retention. Aβ was cleared twofold faster in the sleeping mice as compared with the awake mice ($n = 23$ to 29 mice, $P < 0.05$, ANOVA with Bonferroni test) (Fig. 3, A and B, $P < 0.05$). Aβ clearance did not differ between sleeping and anesthetized mice. Because Aβ is also removed from CNS via receptor-mediated transport across the blood-brain barrier (*24*), we also analyzed the clearance of an inert tracer, ^{14}C-inulin. ^{14}C-inulin was cleared more efficiently (greater than twofold) in sleeping and anesthetized mice as compared with awake mice (Fig. 3, C and D).

What drives the brain state–dependent changes of the interstitial space volume? The observation that anesthesia increases glymphatic influx and efflux (Figs. 1 and 3), suggests that it is not circadian rhythm but rather the sleep-wake state itself that determines the volume of the interstitial space and therefore the efficiency of glymphatic solute clearance. Arousal is driven by the concerted release of neuromodulators (*25*). In particular, locus coeruleus–derived noradrenergic signaling appears critical for driving cortical networks into the awake state of processing (*26*, *27*). In peripheral tissues, such as kidney and heart, noradrenaline regulates the activity of membrane transporters and channels that control cell volume (*28*). We hypothesized that adrenergic signaling in the awake state modifies cell volume and thus the size of the interstitial space. We first assessed whether suppression of adrenergic signaling in the awake conscious brain can enhance glymphatic tracer influx by pretreating awake mice with a cocktail of adrenergic receptor antagonists or vehicle (aCSF) 15 min before infusion of fluorescent CSF tracers (*27*). The adrenergic receptor antagonists were administered through a cannula inserted into the cisterna magna, with an initial bolus followed by slow continuous drug infusion. Administration of adrenergic antagonists induced an increase in CSF tracer influx, resulting in rates of CSF tracer influx that were more comparable with influx observed during sleep or anesthesia than in the awake state (Fig. 4, A and B, and fig. S5). We asked whether increases in the level of norepinephrine (NE) resulting from stress during restraining at the microscope stage affected the observations. Microdialysis samples

of the interstitial fluid showed that the NE concentration did not increase in trained mice during restraining but that NE, as expected, fell after administration of ketamine/xylazine (Fig. 4C).

We next evaluated whether adrenergic receptor inhibition increased interstitial volume in the same manner as sleep and anesthesia. We used the TMA method to quantify the effect of local adrenergic inhibition on the volume of the interstitial space. To restrict adrenergic inhibition to the cortex, receptor antagonists were applied directly to the exposed cortical surface rather than intracisternal delivery. TMA recordings showed that inhibition of adrenergic signaling in cortex increased the interstitial volume fraction from 14.3 ± 5.2% to 22.6 ± 1.2% (n = 4 to 8 mice, P < 0.01, t test). Interstitial volume was significantly greater than in awake littermates exposed to vehicle (aCSF) (P < 0.01) but comparable with the interstitial volume in sleeping or anesthetized mice (P = 0.77 and P = 0.95, respectively, t test) (Fig. 4D). Cortical ECoG displayed an increase in the power of slow waves when exposed to adrenergic receptor antagonists (n = 7 mice, P < 0.01, one-way ANOVA with Bonferroni test). In accordance with earlier findings (*27*), analysis of the power spectrum showed that inhibition of adrenergic signaling transformed the cortical ECoG of awake mice into a more sleep-like, albeit less regular, profile (Fig. 4E). These analyses suggest that adrenergic signaling plays an important role in modulating not only cortical neuronal activity but also the volume of the interstitial space. NE triggers rapid changes in neural activity (*27*, *28*), which in turn can modulate the volume of the interstitial space volume (*29*). Nevertheless, additional analysis is clearly required to determine which cell types contribute to expansion of the interstitial space volume during sleep, anesthesia, or blockade of NE receptors (Figs. 2, B to D, and 4D).

Because of the high sensitivity of neural cells to their environment, it is essential that waste products of neural metabolism are quickly and efficiently removed from the brain interstitial space. Several degradation products of cellular activity, such as Aβ oligomers and amyloid depositions, have adverse effects on synaptic transmission (*30*) and cytosolic Ca^{2+} concentrations (*31*) and can trigger irreversible neuronal injury (*32*). The existence of a homeostatic drive for sleep—including accumulation of a "need to sleep" substance during wakefulness that dissipates during sleep—has been proposed (*33*). Because biological activity is inevitably linked to the production of metabolic degradation products, it is possible that sleep subserves the important function of clearing multiple poten-

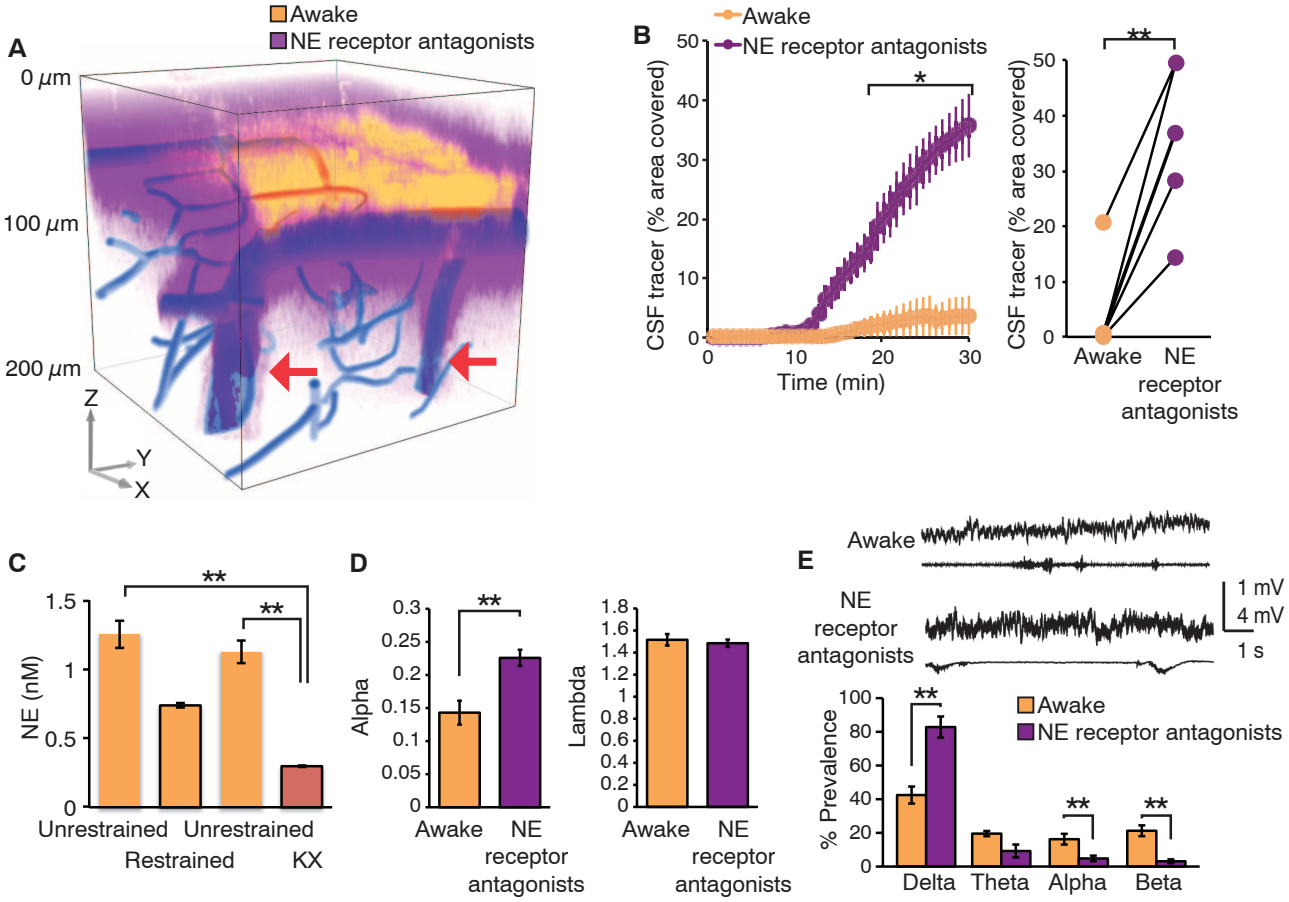

Fig. 4. Adrenergic inhibition increases CSF influx in awake mice. (**A**) CSF tracer influx before and after intracisternal administration of a cocktail of adrenergic receptor antagonists. FITC-dextran (yellow, 3 kD) was first injected in the cisterna magna in the awake mouse, and cortical tracer influx was visualized by means of two-photon excitation for 30 min. The adrenergic receptor antagonists (prazosin, atipamezole, and propranolol, each 2 mM) were then slowly infused via the cisterna magna cannula for 15 min followed by injection of Texas red-dextran (purple, 3 kD). The 3D reconstruction depicts CSF influx 15 min after the tracers were injected in cisterna magna. The vasculature was visualized by means of cascade blue-dextran. Arrows point to penetrating arteries. (**B**) Comparison of tracer influx as a function of time before and after administration of adrenergic receptor antagonists. Tracer influx was quantified in the optical section located 100 μm below the cortical surface; n = 6 mice; *P < 0.05, two-way ANOVA with Bonferroni test. (Right) The tracer intensity during the two arousal states at the 30-min time point was compared. **P < 0.01, t test. (**C**) Comparison of the interstitial concentration of NE in cortex during head-restraining versus unrestrained (before and after), as well as after ketamine/xylazine anesthesia. Microdialysis samples were collected for 1 hour each and analyzed by using high-performance liquid chromatography. **P < 0.01, one-way ANOVA with Bonferroni test. (**D**) TMA^+ iontophoretic quantification of the volume of the extracellular space before and after adrenergic inhibition; n = 4 to 8 mice; **P < 0.01, t test. (**E**) Power spectrum analysis, n = 7 mice; **P < 0.01, one-way ANOVA with Bonferroni test.

tially toxic CNS waste products. Our analysis indicates that the cortical interstitial space increases by more than 60% during sleep, resulting in efficient convective clearance of Aβ and other compounds (Figs. 2 and 3). The purpose of sleep has been the subject of numerous theories since the time of the ancient Greek philosophers (*34*). An extension of the findings reported here is that the restorative function of sleep may be due to the switching of the brain into a functional state that facilitates the clearance of degradation products of neural activity that accumulate during wakefulness.

References and Notes

1. C. B. Saper, P. M. Fuller, N. P. Pedersen, J. Lu, T. E. Scammell, *Neuron* **68**, 1023–1042 (2010).
2. J. A. Hobson, *Nature* **437**, 1254–1256 (2005).
3. B. A. Malow, *Epilepsy Curr.* **4**, 193–195 (2004).
4. R. Stickgold, *Nature* **444**, 559–560 (2006).
5. A. Rechtschaffen, M. A. Gilliland, B. M. Bergmann, J. B. Winter, *Science* **221**, 182–184 (1983).
6. P. J. Shaw, G. Tononi, R. J. Greenspan, D. F. Robinson, *Nature* **417**, 287–291 (2002).
7. P. Montagna, P. Gambetti, P. Cortelli, E. Lugaresi, *Lancet Neurol.* **2**, 167–176 (2003).
8. J. R. Cirrito *et al.*, *Neuron* **48**, 913–922 (2005).
9. M. E. Larson *et al.*, *J. Neurosci.* **32**, 10253–10266 (2012).
10. K. Yamada *et al.*, *J. Neurosci.* **31**, 13110–13117 (2011).
11. K. Aukland, R. K. Reed, *Physiol. Rev.* **73**, 1–78 (1993).
12. J. J. Iliff *et al.*, *Sci. Transl. Med.* **4**, 147ra111 (2012).
13. J. J. Iliff *et al.*, *J. Clin. Invest.* **123**, 1299–1309 (2013).
14. M. Nedergaard, *Science* **340**, 1529–1530 (2013).
15. R. J. Bateman *et al.*, *Nat. Med.* **12**, 856–861 (2006).
16. J. E. Kang *et al.*, *Science* **326**, 1005–1007 (2009).
17. C. Nicholson, J. M. Phillips, *J. Physiol.* **321**, 225–257 (1981).
18. C. Nicholson, *J. Neurosci. Methods* **48**, 199–213 (1993).
19. X. Yao, S. Hrabetová, C. Nicholson, G. T. Manley, *J. Neurosci.* **28**, 5460–5464 (2008).
20. C. Nicholson, E. Syková, *Trends Neurosci.* **21**, 207–215 (1998).
21. E. Syková, C. Nicholson, *Physiol. Rev.* **88**, 1277–1340 (2008).
22. E. Syková *et al.*, *Proc. Natl. Acad. Sci. U.S.A.* **102**, 479–484 (2005).
23. J. P. Kinney *et al.*, *J. Comp. Neurol.* **521**, 448–464 (2013).
24. R. Deane *et al.*, *J. Clin. Invest.* **118**, 4002–4013 (2008).
25. M. Steriade, D. A. McCormick, T. J. Sejnowski, *Science* **262**, 679–685 (1993).
26. M. E. Carter *et al.*, *Nat. Neurosci.* **13**, 1526–1533 (2010).
27. C. M. Constantinople, R. M. Bruno, *Neuron* **69**, 1061–1068 (2011).
28. J. O'Donnell, D. Zeppenfeld, E. McConnell, S. Pena, M. Nedergaard, *Neurochem. Res.* **37**, 2496–2512 (2012).
29. C. J. McBain, S. F. Traynelis, R. Dingledine, *Science* **249**, 674–677 (1990).
30. K. Parameshwaran, M. Dhanasekaran, V. Suppiramaniam, *Exp. Neurol.* **210**, 7–13 (2008).
31. K. V. Kuchibhotla *et al.*, *Neuron* **59**, 214–225 (2008).
32. M. P. Mattson, *Ann. N. Y. Acad. Sci.* **747**, 50–76 (1994).
33. A. Borbely, I. Tobler, in *Brain Mechanisms of Sleep*, D. J. McGinty, Ed. (Raven, New York, 1985), pp. 35–44.
34. J. Barbera, *Sleep Med.* **9**, 906–910 (2008).

Acknowledgments: This study was supported by NIH/National Institute of Neurological Disorders and Stroke (NS078167 and NS078304 to M.N. and NS028642 to C.N.). We thank S. Veasey for comments on the manuscript.

Supplementary Materials

www.sciencemag.org/content/342/6156/373/suppl/DC1
Materials and Methods
Figs. S1 to S5
References

30 May 2013; accepted 28 August 2013
10.1126/science.1241224

Reading Literary Fiction Improves Theory of Mind

David Comer Kidd* and Emanuele Castano*

Understanding others' mental states is a crucial skill that enables the complex social relationships that characterize human societies. Yet little research has investigated what fosters this skill, which is known as Theory of Mind (ToM), in adults. We present five experiments showing that reading literary fiction led to better performance on tests of affective ToM (experiments 1 to 5) and cognitive ToM (experiments 4 and 5) compared with reading nonfiction (experiments 1), popular fiction (experiments 2 to 5), or nothing at all (experiments 2 and 5). Specifically, these results show that reading literary fiction temporarily enhances ToM. More broadly, they suggest that ToM may be influenced by engagement with works of art.

The capacity to identify and understand others' subjective states is one of the most stunning products of human evolution. It allows successful navigation of complex social relationships and helps to support the empathic responses that maintain them (*1*–*5*). Deficits in this set of abilities, commonly referred to as Theory of Mind (ToM), are associated with psychopathologies marked by interpersonal difficulties (*6*–*8*). Even when the ability is intact, disengagement of ToM has been linked to the breakdown of positive interpersonal and intergroup relationships (*9*).

Researchers have distinguished between affective ToM (the ability to detect and understand others' emotions) and cognitive ToM (the inference and representation of others' beliefs and intentions) (*7*, *8*). The affective component of ToM, in particular, is linked to empathy (positively) and antisocial behavior (negatively) (*7*, *8*). It is thus not surprising that we foster ToM in our children by having them attend to the emotional states of others: "Do you think he is happy or sad as a consequence of your action?" Such explicit encouragements to understand others usually diminish when children appear to skillfully and empathically engage in interpersonal relationships. Cultural practices, though, may function to promote and refine interpersonal sensitivity throughout our lives. One such practice is reading fiction.

Familiarity with fiction, self-reported empathy, and performance on an advanced affective ToM test have been correlated (*10*, *11*), and limited experimental evidence suggests that reading fiction increases self-reported empathy (*12*, *13*). Fiction seems also to expand our knowledge of others' lives, helping us recognize our similarity to them (*10*, *11*, *14*). Although fiction may explicitly convey social values and reduce the strangeness of others, the observed relation between familiarity with fiction and ToM may be due to more subtle characteristics of the text. That is, fiction may change how, not just what, people think about others (*10*, *11*, *14*). We submit that fiction affects ToM processes because it forces us to engage in mind-reading and character construction. Not any kind of fiction achieves that, though. Our proposal is that it is literary fiction that forces the reader to engage in ToM processes.

The category of literary fiction has been contested on the grounds that it is merely a marker of social class, but features of the modern literary novel set it apart from most best-selling thrillers or romances. Miall and Kuiken (*15*–*17*) emphasize that through the systematic use of phonological, grammatical, and semantic stylistic devices, literary fiction defamiliarizes its readers. The capacity of literary fiction to unsettle readers' expectations and challenge their thinking is also reflected in Roland Barthes's (*18*) distinction between writerly and readerly texts. Although readerly texts—such as most popular genre fiction—are intended to entertain their mostly passive readers, writerly—or literary—texts engage their readers creatively as writers. Similarly, Mikhail Bakhtin (*19*) defined literary fiction as polyphonic and proposed that readers of literary fiction must contribute their own to a cacophony of voices. The absence of a single authorial perspective prompts readers to enter a vibrant discourse with the author and her characters.

Bruner (*20*), like Barthes and Bakhtin, has proposed that literature engages readers in a discourse that forces them to fill in gaps and search "for meanings among a spectrum of possible meanings" (p. 25). Bruner argues that to elicit

The New School for Social Research, 80 Fifth Avenue, New York, NY 10011, USA.

*Corresponding author. E-mail: kiddd305@newschool.edu (D.C.K.); castanoe@newschool.edu (E.C.)

www.sciencemag.org/content/full/342/6156/373/suppl/DC1

Supplementary Material for

Sleep Drives Metabolite Clearance from the Adult Brain

Lulu Xie, Hongyi Kang, Qiwu Xu, Michael J. Chen, Yonghong Liao, Meenakshisundaram Thiyagarajan, John O'Donnell, Daniel J. Christensen, Charles Nicholson, Jeffrey J. Iliff, Takahiro Takano, Rashid Deane, Maiken Nedergaard*

*Corresponding author. E-mail: nedergaard@urmc.rochester.edu

Published 18 October 2013, *Science* **342**, 373 (2013)
DOI: 10.1126/science.1241224

This PDF file includes:

Sleep Drives Metabolite Clearance from the Adult Brain

Xie et al., Manuscript 1241224

Supplementary Materials and Methods

All experimental data were collected in male C57/BL6 mice (Charles River, 10-12 weeks). The experiments were approved by the Institution of Animal Care and Use Committee of University of Rochester and efforts were taken to minimize the number of animals used.

2-photon imaging of CSF tracer influx

For in vivo imaging, mice were anesthetized with 2% isoflurane and a head plate was glued to the skull. The mice were habituated to the microscope stage over the next 2 days during 3-4 training sessions each lasting 30-60 min. At day 3, the animals were again anesthetized with 2% isoflurane and a cranial window was prepared over the right hemisphere at 2.5 mm lateral and 2 mm posterior to bregma. Dura was left intact and the craniotomy (~3 mm diameter) was filled with aCSF and covered with a modified glass coverslip, then sealed with dental cement. A small burr hole was prepared for ECoG recordings over the left hemisphere mirroring the position of the cranial window (2.5 mm lateral and 2 mm posterior to bregma). A 30GA needle was implanted into the cisterna magna and glued to the skull with dental cement. The open end of the needle was inserted into a piece of polyethylene tubing, which was sealed by cauterization. Custom-made EMG leads were inserted in the neck muscle and secured with sutures. All animals were allowed to recover for 4-6 hrs prior to imaging.

To compare arousal state transitions, CSF tracer influx was imaged in 3 different groups: (1) animals that were initially asleep and subsequently woken up by gentle movement of their tails. These imaging data were collected when mice were naturally asleep (12-2 pm). (2) Awake mice that were anesthetized with a mixture of 100 mg/kg ketamine and 10 mg/kg xylazine i.p. These experiments were performed when the mice were naturally awake (8-10 pm). (3) Awake mice in which a mixture of norepinephrine receptor antagonists was administered via the cisterna magna cannula. These experiments were performed at 8-10 pm. The state of brain activity was monitored by ECoG in the contralateral hemisphere and by an EMG electrode

inserted into the neck muscle. The tails of the mice were gently handled during the awake state in all three groups to prevent spontaneous sleep.

To establish the effect of the arousal state on CSF influx, Texas red or FITC labeled dextran with identical molecular weight (3kD, constituted in aCSF at a concentration of 0.5%) were infused up to a total volume of 5 µl at a rate of 1µl/min over 5 minutes with a syringe pump. CSF tracer was administered via cisterna magna using a two-way divider fitted to the polyethylene tubing. To visualize the vasculature, the BBB impermeable cascade blue-dextran (MW 10 kD, 1% in saline,) was injected i.v. via the femoral vein. A Ti:Sapphire laser, FV300 laser-scanning system controlled by Fluoview software and an upright microscope were used for *in vivo* imaging as described previously (*1*). A 20X water immersion lens was used to image tracer influx and the cerebral vasculature. FITC and Texas Red were excited using 820 nm, whereas 800 nm excitation was used for cascade Blue. Red (590-650nm), green (500-550nm), and blue (403-427nm) bandpass filters were used to collect emission fluorescence from Texas Red, FITC, and cascade Blue, respectively. The experiments were designed such that CSF tracer influx could be quantified in two different stages of brain activity in the same mouse: 1) cortical influx of the CSF tracer (alternating FITC- or Texas Red-dextran) was imaged for a total of 30 min, followed by 2) a transition to a different state of brain activity (e.g., sleep to awake; awake to anesthesia; or awake followed by administration of norepinephrine receptor antagonists). The second CSF tracer was infused 15 minutes later and CSF influx imaged for another 30 min. Cortex was repeatedly scanned from the surface to 200 µm below the surface at 1 min intervals using 5 µm z-steps and 512 x 512 pixel resolution during the 30 min imaging session. ImageJ software with the UCSD plugin set was used for data analysis. Optical sections located 100 µm below the cortical surface were selected for the analysis of the kinetics of CSF tracer influx. To define tracer coverage (glymphatic influx), the area (μm^2) of the optical section with a pixel intensity > 40 (out of 255) was quantified. This area was expressed as the percentage of total area of the optical section. To define perivascular tracer movement, circular regions of interest (ROI) 25 pixels in diameter were defined surrounding penetrating arteriole. To define the exchange of perivascular CSF tracer with interstitial fluid (ISF) of the surrounding parenchyma, donut-shaped ROIs were defined that had an external diameter of 150 pixels and an internal

diameter of 50 pixels. Respectively, these ROIs corresponded to the approximate dimensions of the arteriole plus perivascular regions and a small arbitrary portion of the adjacent parenchyma tissue, thus allowing the exclusion of the perivascular tracer from quantification of pixel intensity, to gain a measure of exchange. The ROIs were centered upon penetrating arterioles. Mean pixel intensity within these ROIs was measured at each time point. When tracer movement along penetrating arterioles, or into peri-arterial brain tissue was compared, a 2-way ANOVA was used followed by Bonferroni's post-hoc test. A 2-way ANOVA was used to compare the differences followed by Bonferroni's post-hoc test. Penetrating arterioles were distinguished from penetrating venules on the basis of the direction of flow as well as morphology: surface arteries are positioned superficially to surface veins and exhibit less branching at superficial cortical depths. For 3D visualization, cascade blue-labeled vasculature was imaged with higher resolution of 0.7 x 0.7 x 0.7 µm voxel size. The vasculature was traced and reconstructed using Neurolucida software. Images of CSF tracers captured at 15 min after cisterna magna administration of the tracers were reconstructed in 3D with Neurolucida and color-coded before merging the the 3D reconstruction of the vasculature.

The mixture of norepinephrine receptor antagonists (prazosin, atipamezole and propranolol, all at 2 mM) (*2*) was injected into cisterna magna starting with a bolus of 5 µl at a rate of 1µl/min followed by a slower infusion rate of 0.167 µl/min with a syringe pump until the end of experiment.

EEG, ECoG, and EMG recordings and analysis

Cortical EEG (ECoG) was recorded by insertion of a single barrel electrode (tip diameter of 2-3 µm) 2.5 mm lateral and 2 mm posterior to bregma to a depth of 150 µm in the contralateral hemisphere to the window prepared for 2-photon imaging to avoid penetrating the ipsilateral dura, which can alter CSF tracer fluxes (*3*). ECoG and EMG activity were co-currently recorded and compared in awake, sleeping, and anesthetized animals (**Fig. S1**). In all experiments measuring the interstitial space, ECoG was recorded by the reference barrel of the TMA microelectrode. In either case the signals were collected with Clampex 10.2 and broken down into artifact-free 5 min epochs, These epochs were further broken down into the % prevalence

of Delta (0 – 4 Hz), Theta (4 – 7 Hz), Alpha (8 – 13 Hz), and Beta (13 – 20 Hz) power bands as previously described (*4-6*). Wakefulness was defined as desynchronized low-amplitude ECoG, while sleep states were defined as synchronized high amplitude activity dominated by low frequency waves (0-4 Hz) in artifact-free five minute epochs.

To assess whether the microelectrode recordings of ECoG were representative of standard EEG recordings, we compared ECoG to EEG recordings obtained by commercial telemetric electrodes. The headplate was mounted under 2% isoflurane anesthesia, and small burr holes were drilled in the skull 2.5 mm lateral and 2 mm posterior to bregma on either side of the midline. EEG wire leads were then inserted into the burr holes on one side of the midline between the skull and underlying dura. EEG leads were secured with dental acrylic. An EMG lead was inserted in the neck muscle. The animals were allowed to recover for 24 hrs, then glass electrodes used for ECoG were inserted in the contralateral burr holes to obtain dual recordings of cortical activity, as well as EMG (*7-9*).

Sleep versus wakefulness was manually scored by visual inspection of the mice behavior every 5 min in radiolabeled clearance studies to avoid contamination of the equipment. Mice in the awake group were kept alert by gentle manipulation of their cages.

Iontophoretic tetramethylammonium (TMA) quantification of the interstitial space volume

All experimental procedures were adapted from the previous studies(*10*) (*11*). The single barrel iontophoresis microelectrode (tip diameter of 2-3 **µ**m) contained 150 mM TMA-chloride and 10 µM Alexa 488. A serials of currents of 20 nA, 40 nA and 80 nA were be applied by a dual-channel microelectrode preamplifier. For measurements of TMA, microelectrodes with an outer diameter of 2–3 µm were fabricated from double-barreled theta-glass using a tetraphenylborate-based ion exchanger. The TMA barrel was backfilled with 150 mM TMA-chloride, whereas the reference barrel contained 150 mM NaCl and 10 µM Alexa 568. All recordings were obtained by inserting the two electrodes to a depth of 150 µm below the cortical surface. Recording electrodes were inserted 2.5 mm lateral and 2 mm posterior to bregma or in the same location as the CSF tracer imaging analysis. The electrode tips were imaged after insertion using 2-photon excitation to determine the exact distance between the

electrodes (typically ~150 µm). The TMA signal was calculated by subtracting the voltage measured by the reference barrel from the voltage measured by the ion-detecting barrel using a dual-channel microelectrode preamplifier. The Nikolsky equation was used for calibration of the TMA electrodes based on measurements obtained in electrodes containing 0.5, 1, 2, 4, and 8 mM TMA-chloride in 150 mM NaCl. The TMA measurements were acquired relative to similar recordings obtained in 0.3% agarose prepared from a solution containing 0.5 mM TMA and 150 mM NaCl. A custom-made MatLab software, 'Walter', developed by C. Nicholson was used to calculate α and λ values (*10*). The mixture of norepinephrine receptor antagonists (prazosin, atipamezole and propranolol, all at 25 µM) (*2*) were dissolved in aCSF and applied at the surface of the brain in the experiments involving recordings of interstitial space using TMA microelectrodes. Due to the small volume administered of CSF administered in cisterna magna, higher concentrations of the NE receptor antagonists (2 mM) where used in experiments involving CSF tracer imaging.

Microdialysis and norepinephrine analysis of dialysate

To evaluate the norepinephrine level in mouse brain under different conditions, a dialysis guide cannula was positioned within cortex, the location of the cannula tip was AP + 2.0, ML + 0.3 from bregma and DV -1.0 from dura. The guide cannula was secured to the skull with dental cement. After implantation, animals were allowed to recover for at least 24 hours and were then training for head restraint as described above. Dialysis probe was inserted into the cannula and perfused with filtered aCSF (145 mM NaCl, 2.7 mM KCl 1.2 mM $CaCl_2$ 2mM Na_2HPO_4 and 1.0 mM $MgCl_2$, adjusted to pH 7.4) at a rate of 0.33 µl/min for 12 hours. On test day, dialysate samples were obtained from mice at 1 hr intervals while either freely moving in their cage (unrestrained), restrained, followed by another 1 hr period of free movement in their cage (unrestrained). Finally, the animals were anesthetized with ketamine/xylazine and the last 1 hr microdialysis sample collected. The 20 µl dialysates were immediately analyzed by HPLC-EC system consisting of an ESA 584 pump, an ESA MD-160, 1.5x250 mm, 5 µM column, and an ESA 5600A Coulochem II detector with an ESA 5041 analytical cell(+ 220v). The mobile phase consisted of 150 mM ammonium acetate, 140 µM EDTA, 15% methanol (vol/vol), and 5%

Acetonitrile with a pH of 6.0, which was filtered and degassed prior to use. The flow rate through the system was 0.15 ml/min.

Radiolabeled tracer influx and clearance

To evaluate the absolute proportion of subarachnoid CSF that enters the brain, radio-labeled ^{3}H-mannitol (0.1 µCi) was delivered intracisternally. After 15, 30 or 45 min, animals were rapidly decapitated, the skull opened, the dura removed and the brain harvested. The brain was solubilized in 2 ml Soluene at 45^{o}C overnight. 10 ml Hionic Fluor liquid scintillation cocktail was added and radioactivity was measured in a Multipurpose Scintillation Counter. Brain radioactivity was normalized to total radioactivity detected in a 10 µl aliquot transferred directly into a scintillation vial immediately before intracisternal radio-tracer injection and expressed as the % of total injected radioactivity. ^{3}H-mannitol accumulation in the brain was compared by 2-way ANOVA with Bonferroni's post-hoc test.

To evaluate the rates of interstitial fluid and solute clearance from the brain, radio-labeled tracers (^{125}I-Aβ_{1-40} and ^{14}C-inulin) were injected stereotactically into the brain parenchyma. Radio-iodinated Aβ was used since there was no significant difference between the clearances of Aβ from brain using radio-iodinated Aβ or non-radio labeled Aβ (ELISA) (*12*). Briefly, a stainless steel guide cannula was implanted into the right frontal cortex of anesthetized 10-12 weeks old male mice (2% isoflurane) with the coordinates of the cannula tip at 0.7 mm anterior and 3.0 mm lateral to the bregma, and 1.3 mm below the surface of the brain. Animals were allowed to recover after surgery and the experiments performed 12-24 hrs after the guide tube cannulation, as reported previously (*13, 14*). Clearance of Aβ and inulin were studied under three conditions: anesthetic (100 mg/kg ketamine and 10 mg/kg xylazine) (23 mice), awake (25 mice) and sleeping (29 mice). In each mouse, a small volume of mock CSF (0.5 µL), containing ^{125}I-labeled Aβ (10 nM monomer ^{125}I-Aβ_{1-40}) and tracer levels of ^{14}C-inulin (0.05 µCi), was simultaneously injected (33 GA cannula) into brain ISF over 5 minutes. At the end of the experiments (predetermined time-points between 10 and 240 min) the brain was removed and prepared for radioactivity analysis and TCA analyses of Aβ (*14*). Studies with ^{125}I-labeled Aβ have demonstrated that radiolabeled Aβ remains mainly intact in brain ISF (> 95%) within 300

min of *in vivo* clearance studies (*15*). ^{125}I radio-activities were determined using a gamma counter. For ^{14}C counting, the samples were solubilized in 0.5 ml tissue solubilizer overnight, followed by addition of 5 ml of scintillation cocktail and analyzed in a liquid scintillation counter. *Calculations of clearance rates:* The percentage of radioactivity remaining in the brain after microinjection was determined as % recovery in brain = 100 x (N_b/N_i) (eq. 1), where, N_b is the radioactivity remaining in the brain at the end of the experiment and N_i is the radioactivity injected into the brain ISF, i.e., the d.p.m. for ^{14}C-inulin and the c.p.m. for the TCA-precipitable ^{125}I-radioactivity. Inulin was used as a metabolically inert polar molecule which is neither transported across the BBB nor retained by the brain; its clearance rate provides a measure of the ISF bulk flow and was calculated as N_B (inulin)/N_i(inulin) = exp (- k inulin * t) (eq. 2). The total clearance of Aβ40 was determined using a similar equation. Rate constants and half-time (t1/2) were determined using Prism version 3. Clearance data were analyzed using 2-way ANOVA and Bonferroni's post-hoc test to determine differences at individual time points.

Supplementary Figures

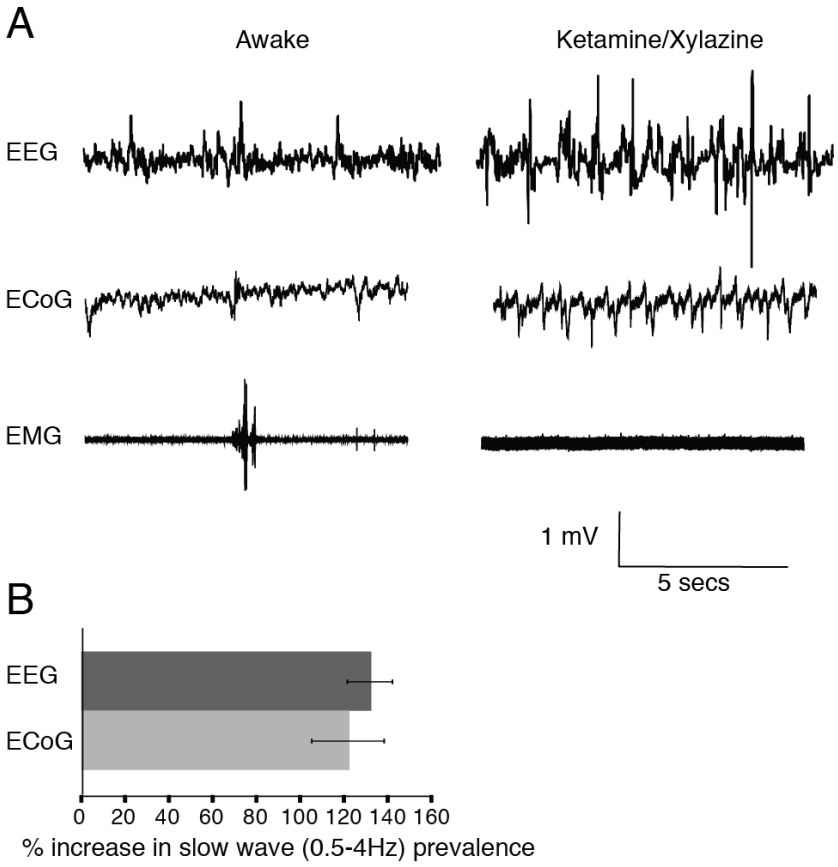

Fig. S1. Validation of Sleep/Wake Scoring

Standard EEG electrodes are fairly large (1-2 mm) and rest on top of the dura. To avoid interference with CSF convective fluxes in the subarachnoid space due to placement of EEG electrodes, ECoG was recorded in combination with EMG in all in vivo 2-photon imaging experiments. To evaluate how accurately ECoG/EMG recordings detect transitions in the arousal state, standard EEG recordings were compared to cortical ECoG recordings obtained in the same animals. (**A**) Standard EEG electrodes were positioned over the left hemisphere (2.5 mm lateral and 2 mm posterior to bregma) the day before the experiments. ECoG recordings were collected by inserting a glass micropipette 150 µm below the pial surface in the right hemisphere (2.5 mm lateral and 2 mm posterior to bregma). The EMG electrode was inserted in the neck muscles. (**B**) Comparison of percentage increase in slow wave prevalence upon transition from awake to ketamine/xylazine anesthesia using standard EEG electrodes and ECoG recordings (n = 5).

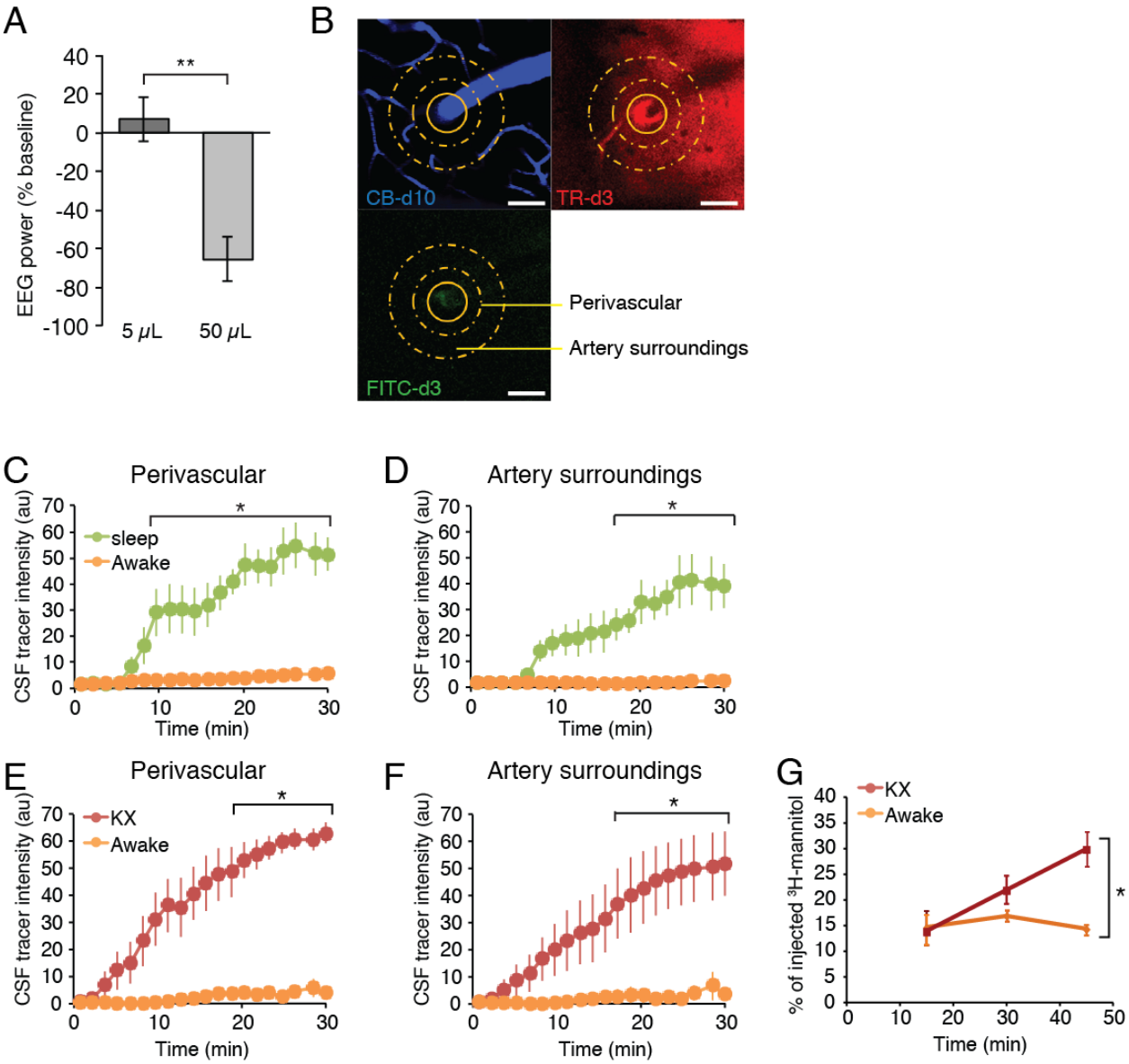

Fig. S2. Effect of intracisternal injection on ECoG and comparison of perivascular and parenchymal CSF tracer influx in two different arousal states in the same animal.

(A) Analysis of the effect of intracisternal injection of artificial cerebrospinal fluid on (aCSF) ECoG power. The aCSF contained TR-d3 and FITC-d3 (both 5%) and was injected at a rate of 1 µl/min. Injecting 5 µl was not associated with changes in EcoG power, whereas the 50 µl injections triggered a transient dampening of ECoG signal amplitude (*P < 0.05 One-Way ANOVA with Tukey Post hoc test). **(B)** To establish the effect of the arousal state on CSF tracer influx kinetics, Texas red or FITC labeled dextran with identical molecular weight (3kD) were injected in cisterna magna in the same animal during two different arousal states. We

compared the influx of Texas red (TR-d3) and FITC (FITC-d3) dextran in sleeping mice and then again after waking them up by gentle movement of their tail. These experiments were done when mice are naturally asleep (12-2pm). In another group of mice, tracer influx in awake mice was compared to tracer influx after the mice were anesthetized with ketamine/xylazine. These experiments were performed when mice were naturally awake (8-10pm). Tracer influx was analyzed along peri-arterial pathways and in the cortical parenchyma using in vivo 2-photon laser scanning microscopy through a closed cranial window. The cerebral vasculature was visualized via intravenous injection of Cascade Blue-dextran-10 (CB-d10) and penetrating arterioles were identified by morphology and the flow pattern: surface arteries passed superficially to surface veins and exhibited less branching at superficial cortical depths. The Image analysis of intracisternal tracer penetration was conducted with ImageJ software (NIH) with the UCSD plugin set. Imaging planes 100 µm below the cortical surface were selected for the analysis. To define peri-arterial tracer movement, a circular region of interest (ROI, 25 pixels in diameter) was defined surrounding penetrating arteriole (yellow solid circle). To define tracer movement into peri-arterial brain tissue, a donut-shaped ROI was defined that had an external diameter of 150 pixels and an internal diameter of 50 pixels (thus excluding the paravascular ROI, yellow dashed donuts) (*3*). Both circles were centered around penetrating arterioles. Scale bars: 40 µm. (**C-F**) Mean pixel intensity within these ROIs was measured at each time point in XYZT time-lapse movies collected at 5 min intervals. The CSF tracer moved readily into the cortex along penetrating arterioles and into the brain parenchyma in the sleeping and anesthetized state (green and red lines), but not in awake mice (orange line; *$p < 0.05$, $n = 6$ each group). **(G)** Radio labeled ^{3}H-mannitol was injected intracisternally in awake and anesthetized mice. Brains were harvested 15, 30 or 45 min after radio-tracer injection to quantify radiotracer accumulation within the brain parenchyma. Brains were solubilized in Soluene, and total brain count was detected by liquid scintillation counting. Total ^{3}H counts from brain divided by total injected ^{3}H-mannitol were used to calculate CSF influx (*3*). ^{3}H-mannitol accumulated gradually in brain with time in mice anesthetized with ketamine/xylazine, but not significantly in awake mice (*$p < 0.05$, $n = 4$-6 each group, 2-way ANOVA with Bonferroni's post-hoc test).

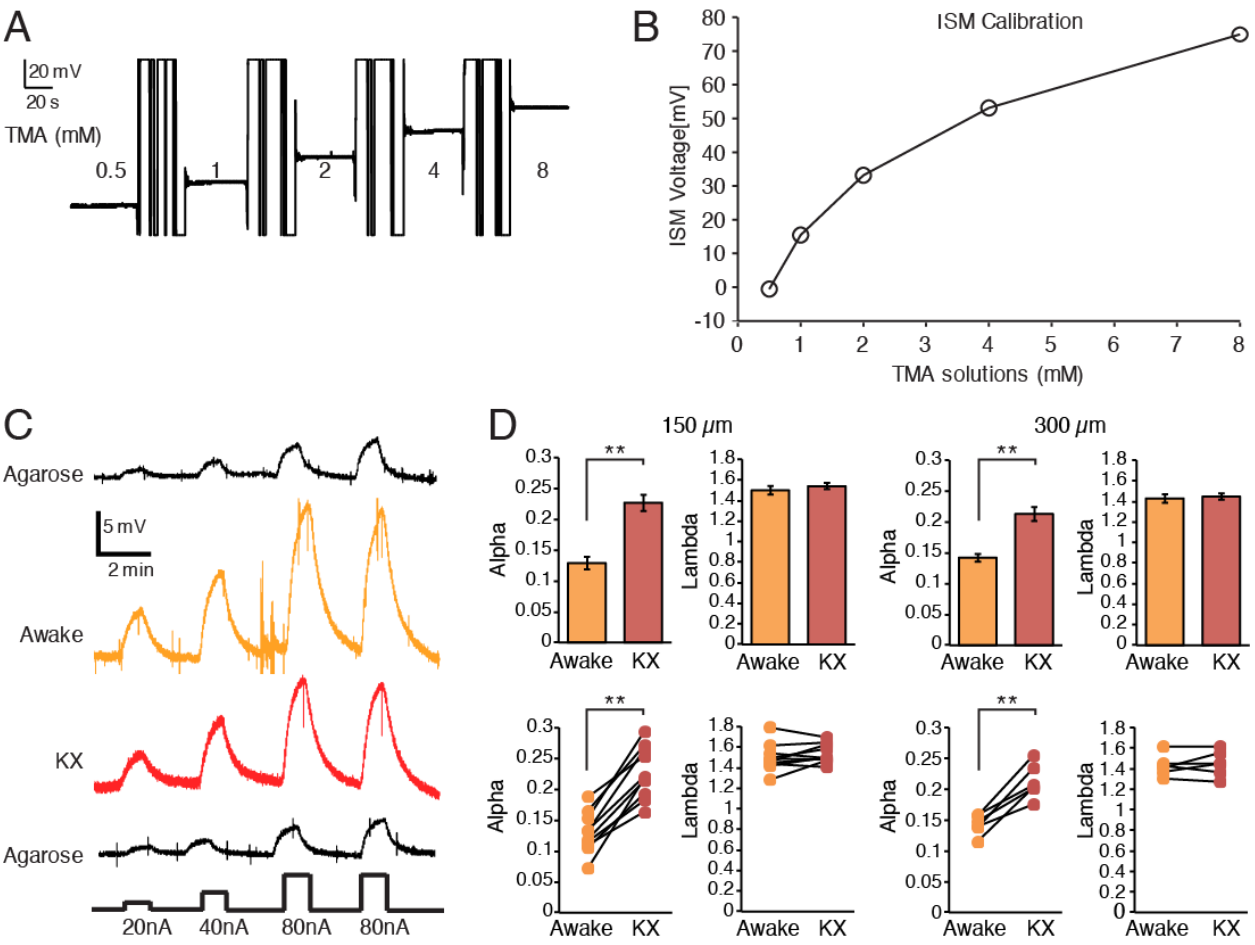

Fig. S3. Measurement of interstitial space volume fraction and tortuosity using the iontophoretic TMA^+ method

(A) TMA-ion selective microelectrodes (ISMs) were calibrated in aCSF solution containing 0.5, 1, 2, 4, and 8 mM TMA-chloride. **(B)** The voltage *versus* the TMA^+ concentration was plotted and fitted to Nikolsky equation (*16*). (**C**) Representative examples of TMA^+ diffusion curves from one experiment in which recordings were first obtained in 1) agorose, 2) awake mouse (150 µm below the cortical surface), 3) same mouse after administration of ketamine/Xylazine (without moving the electrodes), and 4) agarose. Four current injections (20, 40, 80, and 80 nA) were analyzed. (**D**) Alpha and lambda collected at a depth of 150 *versus* 300 µm below the cortical surface did not differ significantly in either the awake or the ketamine/xylazine anesthetized state (n = 10 for 150 µm, n = 6 for 300 µm; ** $p < 0.01$, paired t test).

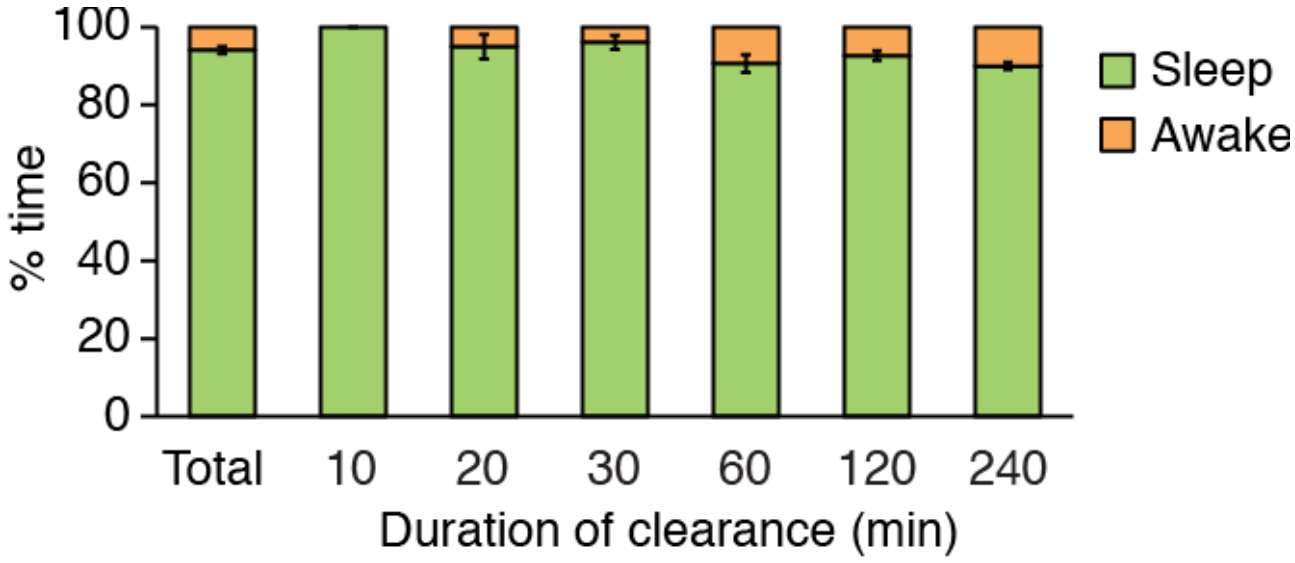

Fig. S4. Sleep scoring for clearance studies

Recordings of ECoG and EMG were not obtained in radiolabeled clearance studies to avoid contaminating the equipment. Instead animals in the awake group were kept alert during the experiments by gentle movement of their cages. Clearance data for sleep was obtained by keeping the room quiet, while an immobilized observer scored the activity state of the mice (sleep versus awake) every 5 min throughout the experiments. The relative amount of sleep in the sleep group during clearance was calculated and plotted. None of the animals in the ketamine/xylazine woke up during the clearance phase (n = 4-27, P = 0.06, one way ANOVA.)

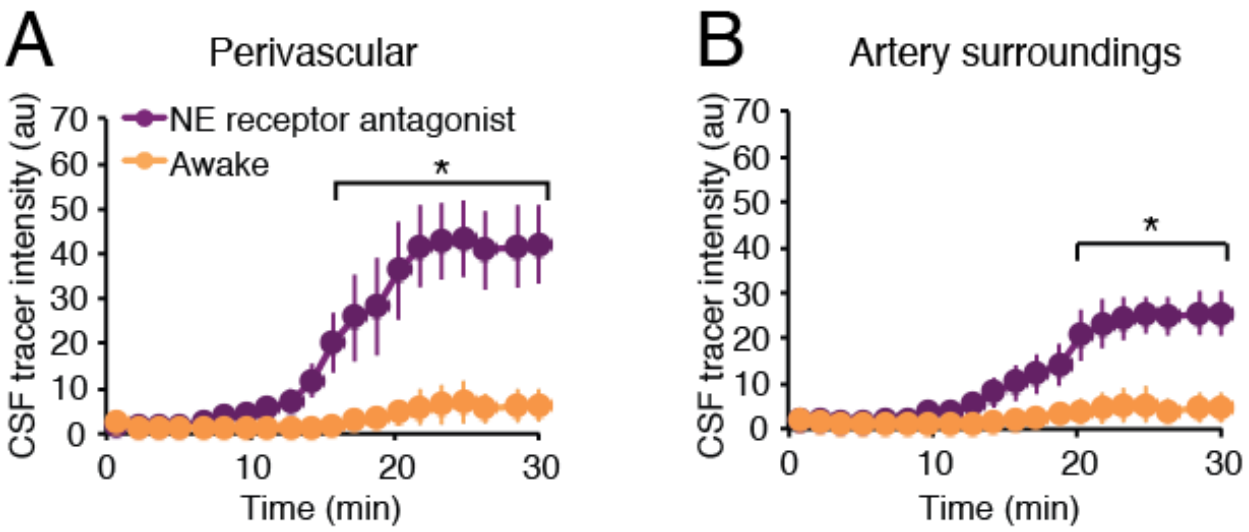

Fig. S5. Intracisternal administration of a mixture of norepinephrine receptor antagonists increases CSF tracer influx.

A mixture of norepinephrine receptor antagonists (prazosin, atipamezole and propranolol, each 2 mM), was injected into the cisterna magna of awake mice starting with a bolus of 5 µl (1µl/min) followed by a constant infusion of 0.167µl/min with a syringe pump until the end of experiment. Using the same approach to detect influx of CSF tracers shown in Fig. S2, the kinetics of tracer influx were compared before and 15 min after NE receptor antagonist administration. Influx of the two dextrans of same molecular weight (TR-d3 and FITC-d3) injected in awake mice orange line prior to administration of norepinephrine receptor antagonists and again 15 min after the injection of the norepinephrine receptor antagonists (purple line) were calculated along peri-arterial pathways and in the cortical parenchyma (*p < 0.05, n= 6 each group, two-way ANOVA with Bonferroni test).

References and Notes

1. X. Wang *et al.*, Astrocytic Ca2+ signaling evoked by sensory stimulation in vivo. *Nature neuroscience* **9**, 816 (Jun, 2006).
2. C. M. Constantinople, R. M. Bruno, Effects and mechanisms of wakefulness on local cortical networks. *Neuron* **69**, 1061 (Mar 24, 2011).
3. J. J. Iliff *et al.*, A Paravascular Pathway Facilitates CSF Flow Through the Brain Parenchyma and the Clearance of Interstitial Solutes, Including Amyloid beta. *Sci Transl Med* **4**, 147ra111 (Aug 15, 2012).
4. G. F. Tian *et al.*, An astrocytic basis of epilepsy. *Nature medicine* **11**, 973 (Sep, 2005).
5. N. A. Oberheim *et al.*, Loss of astrocytic domain organization in the epileptic brain. *The Journal of neuroscience : the official journal of the Society for Neuroscience* **28**, 3264 (Mar 26, 2008).
6. A. S. Thrane *et al.*, General anesthesia selectively disrupts astrocyte calcium signaling in the awake mouse cortex. *Proceedings of the National Academy of Sciences of the United States of America* **109**, 18974 (Nov 13, 2012).
7. E. N. Bruce, M. C. Bruce, S. Vennelaganti, Sample entropy tracks changes in electroencephalogram power spectrum with sleep state and aging. *J Clin Neurophysiol* **26**, 257 (Aug, 2009).
8. K. Hellman, P. Hernandez, A. Park, T. Abel, Genetic evidence for a role for protein kinase A in the maintenance of sleep and thalamocortical oscillations. *Sleep* **33**, 19 (Jan, 2010).
9. H. W. Steenland, V. Wu, H. Fukushima, S. Kida, M. Zhuo, CaMKIV over-expression boosts cortical 4-7 Hz oscillations during learning and 1-4 Hz delta oscillations during sleep. *Mol Brain* **3**, 16 (2010).
10. C. Nicholson, Ion-selective microelectrodes and diffusion measurements as tools to explore the brain cell microenvironment. *Journal of neuroscience methods* **48**, 199 (Jul, 1993).

11. C. Nicholson, Quantitative analysis of extracellular space using the method of TMA+ iontophoresis and the issue of TMA+ uptake. *Can J Physiol Pharmacol* **70 Suppl**, S314 (1992).
12. R. D. Bell *et al.*, Transport pathways for clearance of human Alzheimer's amyloid beta-peptide and apolipoproteins E and J in the mouse central nervous system. *J Cereb Blood Flow Metab* **27**, 909 (May, 2007).
13. J. R. Cirrito *et al.*, P-glycoprotein deficiency at the blood-brain barrier increases amyloid-beta deposition in an Alzheimer disease mouse model. *J Clin Invest* **115**, 3285 (Nov, 2005).
14. R. Deane *et al.*, LRP/amyloid beta-peptide interaction mediates differential brain efflux of Abeta isoforms. *Neuron* **43**, 333 (Aug 5, 2004).
15. R. Deane, A. Sagare, B. V. Zlokovic, The role of the cell surface LRP and soluble LRP in blood-brain barrier Abeta clearance in Alzheimer's disease. *Curr Pharm Des* **14**, 1601 (2008).
16. C. Nicholson, P. Kamali-Zare, L. Tao, Brain Extracellular Space as a Diffusion Barrier. *Computing And Visualization In Science* **14**, 309 (Oct 1, 2011).